Sulfur Poisoning of Electrochemical Reformate Conversion on Ni/Gadolinium-Doped Ceria Electrodes

Matthias Riegraf,[a,*] Michael Philipp Hoerlein,[a] Rémi Costa,[a] Günter Schiller,[a] K. Andreas Friedrich[a]

[a]German Aerospace Centre (DLR), Institute of Engineering Thermodynamics, Pfaffenwaldring 38-40, 70569 Stuttgart, Germany

[*]Corresponding author: E-mail: Matthias.Riegraf@dlr.de, Phone: +49 (0) 711 6862-8027, Fax: +49 (0) 711 6862-747

ABSTRACT

The aim of the present study is the measurement and understanding of sulfur poisoning phenomena in Ni/gadolinium-doped ceria (CGO) based solid oxide fuel cells (SOFC) operating on reformate fuels. The sulfur poisoning behavior of commercial, high-performance electrolyte-supported cells (ESC) with Ni/$Ce_{0.9}Gd_{0.1}O_{2-\delta}$ (CGO10) anodes operated with different fuels was thoroughly investigated by means of current-voltage characteristics and electrochemical impedance spectroscopy, and compared with Ni/Yttria-stabilized zirconia (YSZ) anodes. Various methane- and carbon monoxide-containing fuels were used in order to elucidate the underlying reaction mechanism. The analysis of the cell resistance increase in $H_2/H_2O/CO/CO_2$ fuel gas mixtures revealed that the poisoning behavior is mainly governed by an inhibited hydrogen oxidation reaction at low current densities. At higher current densities, the resistance increase becomes increasingly large, indicating a particularly severe poisoning effect on the carbon monoxide conversion reactions. However, the ability of Ni/CGO anodes to convert carbon monoxide even at H_2S concentration up to 20 ppm was demonstrated, while this was not possible for Ni/YSZ. The sulfur poisoning behavior of Ni/CGO in reformate fuels was fully reversible for short exposure times. From methane steam reforming experiments, it is deduced that the Ni surface is blocked and thus, the water gas shift reaction is fully deactivated as well. However, electrochemical CO oxidation on the CGO surface was shown to be still active. The present results clearly demonstrate that the high sulfur tolerance of Ni/CGO is not only limited to H_2/H_2O fuel systems, but also extends to CO-containing gases.

Keywords: Solid oxide fuel cell (SOFC), anode, degradation, ceria, Ni/GDC, electrochemistry, fuel cells

Introduction

Although continuous progress is achieved with respect to lifetime and performance improvements, solid oxide fuel cells (SOFC) continue to struggle with commercialization. One option to decrease the cost of SOFC systems would be to simplify the balance of plant by reducing the number of upstream fuel processing components, such as the desulfurization unit. However, sulfur-containing impurities in most prospective SOFC fuels such as natural gas and biogas inevitably lead to considerable performance drops upon exposure to Ni-based anodes. Sulfur poisoning of the most commonly used Ni/YSZ cermet anodes has been widely investigated, both experimentally and theoretically, and was related to the Ni surface poisoning with elemental sulfur.[1–7] However, only few studies have targeted the sulfur poisoning behavior of Ni/CGO anodes, although they are used in several commercial applications and were shown to possess a significantly higher sulfur tolerance than Ni/YSZ.[8–18] Hydrogen oxidation on Ni/CGO was frequently assumed to proceed via the same reaction mechanism as on Ni/YSZ, where hydrogen spillover including electrochemical charge transfer at the triple phase boundary (TPB) between Ni/YSZ/gas phase was shown to be the rate-limiting step. However, recent studies of Ni/CGO have suggested that the rate-determining charge transfer reaction is likely to happen at the CGO/gas-phase double layer (DPB) rather than at the TPB between Ni/CGO/gas phase. In these studies, Ni was suggested to act merely as electronic conductor.[19–24] This hypothesis is supported by a number of studies investigating Cu/CGO-based anodes that show high performance, despite the usage of catalytically inactive Cu as the metallic phase.[25,26] This behavior can be explained by the high surface activity of CGO towards H_2 oxidation and its mixed ionic/electronic conductivity (MIEC) at high temperatures and in reducing atmosphere, which originates from the mixed Ce^{3+}/Ce^{4+} oxidation state of cerium.[19,21,22,27,28]

Several research groups have experimentally investigated the influence of sulfur on Ni/CGO-based SOFC operated on H_2/H_2O fuels.[8–14,29,30] Similar to Ni/YSZ anodes, a rapid

initial power output drop occurs already for H_2S concentrations in the ppm level and levels off at H_2S concentrations of approximately 20 ppm.[8,13,29] However, the associated resistance increase for Ni/CGO anodes was significantly less severe. Furthermore, the poisoning behavior was shown to be completely reversible for H_2S concentrations below 100 ppm.[29,31] Hypothetic explanations of this high sulfur tolerance include the activity of CGO as a hydrogen oxidation catalyst in the Ni/CGO system,[19–24] the oxidation of sulfur to SO_2 involving an oxygen spillover from CGO to Ni,[8,12,32] and sulfur diffusion from the surface to the CGO bulk phase.[33,34] While the actual reason still needs to be identified, it is clear that the influence of sulfur on Ni/CGO anodes has to be reevaluated under the assumption that the underlying mechanism might be fundamentally different to Ni/YSZ. In order to make mechanistic conclusions, a more detailed investigation of sulfur poisoning on Ni/CGO is necessary.

With regards to sulfur poisoning in hydrocarbon-containing fuels, a variety of studies has been dedicated to the investigation of Ni/YSZ anodes operating on methane,[6,35–37] reformates,[5] syn-[38,39] and biogas.[40] In order to achieve high efficiencies, SOFC are ideally operated in an internal methane reforming mode. This involves a number of catalytic reactions, which on Ni/YSZ are catalyzed on the Ni surface. The main catalytic reactions are.

$$\text{Methane steam reforming: } CH_4 + H_2O \rightleftharpoons CO + 3H_2 \quad (1)$$

$$\text{Methane dry reforming: } CH_4 + CO_2 \rightleftharpoons 2CO + 2H_2 \quad (2)$$

$$\text{Water gas shift reaction: } CO + H_2O \rightleftharpoons CO_2 + H_2 \quad (3)$$

$$\text{CO oxidation: } CO + O \rightleftharpoons CO_2 \quad (4)$$

From an elementary kinetic point of view, all of these chemical processes are based on identical elementary steps.[6,41,42] Thus, the reactions cannot be seen as independent reaction pathways, as they are inherently coupled in a complex reaction mechanism.

On Ni/YSZ anodes, electrochemical CO oxidation (Eq. 5) was shown to be one order of magnitude slower than electrochemical hydrogen oxidation and the water gas shift reaction due to the slow oxygen spillover charge transfer reaction.[43–46]

Electrochemical CO oxidation: $CO + O^{2-} \rightleftharpoons CO_2 + 2e^-$ (5)

Approaching more realistic operating conditions, several experimental studies have examined the sulfur poisoning of Ni/YSZ anodes operated on $CO/CO_2/H_2/H_2O$ gas mixtures in order to extract detailed information about the influence of sulfur on the water gas shift reaction. [5,39,47] The results of these studies show that the water gas shift reaction is also affected more strongly than the electrochemical oxidation of hydrogen. Thus, mass transport limitation is reached at lower current densities than under sulfur-free conditions. For H_2S concentrations of >20 ppm, both the water gas shift reaction and the methane steam reforming were even shown to be completely deactivated.[37,39]

However, such detailed investigations about the sulfur influence on hydrocarbon-fueled SOFC still have not been carried out for Ni/CGO anodes, although CGO was reported to display a high electro-catalytic activity towards CO oxidation in a number of studies, indicating the possibility of high CO oxidation rates also on Ni/CGO anodes.[10,48,49] Furthermore, the possibility of direct electro-catalytic methane oxidation on Ni/CGO, especially at low steam/carbon ratios, was shown, which is not favorable on Ni/YSZ.[50–52] Moreover, the hypothesized sulfur oxidation opens up the possibility of an at least partly active water gas shift reaction.

Recently, a detailed analysis of sulfur poisoning on Ni/CGO operating on H_2/H_2O fuels was carried out in our group.[29] However, the extent of sulfur poisoning in carbon monoxide-containing systems is still unclear. The present study evaluates the effect of hydrogen sulfide on the performance of Ni/CGO-based SOFC operating on a number of different reformate fuels and compares the observed behavior with Ni/YSZ anodes. This allows us to decouple the different (electro-)catalytic reactions shown in Eq. 1–5 and draw several mechanistic conclusions about the behavior of Ni/CGO anodes.

Experimental Methodology

Two different kinds of commercial, electrolyte-supported SOFC (ESC) were investigated, both based on 160 µm thick 10Sc1CeSZ ($(Sc_2O_3)_{0.1}(CeO_2)_{0.01}(ZrO_2)_{0.89}$) electrolytes. The first cell was a "G3" ESC with a 20 µm thick Ni/$Ce_{0.9}Gd_{0.1}O_{2-\delta}$ (CGO10) anode, a 5 µm thick CGO10 adhesion layer between electrolyte and functional anode layer and an LSMM' MIEC cathode manufactured by the Fraunhofer Institute for Ceramic Technologies and Systems (IKTS).[53] It will be referred to as Ni/CGO-based cell in the following. The second cell was a commercial cell by Kerafol employing a 25 µm thick Ni/8YSZ($(Y_2O_3)_{0.08}(ZrO_2)_{0.92}$) anode, a 5µm thick 8 YSZ adhesion layer and an LSM($(La_{0.75}Sr_{0.25})_{0.95}MnO_3$)/10Sc1CeSZ cathode. This cell will be referred to as Ni/YSZ-based cell. The composition of the LSM was $(La_{0.75}Sr_{0.25})_{0.95}MnO_3$. The weight ratio between metallic and ceramic phases in the anodes, and between LSM and 10Sc1CeSZ in the composite cathode of the second cell was 50:50. In both anodes a current collector layer with increased Ni content was utilized. Moreover, the results in this work are compared to recently published experiments of a third cell.[29] This cell employed the exact same materials and geometry as the Ni/CGO10-based cell in the present study, except for using an LSM/10Sc1CeSZ cathode. This cell is referred to as "Ni/CGO-Ref".

The active area of the planar cells was 4 x 4 cm^2 with a total area of 5 x 5 cm^2. The setup for cell testing enables the characterization of up to four cells simultaneously and has been illustrated and described in detail elsewhere.[29,54] Throughout the present work, the hydrogen utilization (FU_{H2}) is used. This value is calculated by dividing the number of electrons going through the external electrical circuit with the maximum number of electrons that can be generated by the hydrogen inlet. Frequently, overall fuel utilization values are used that include both the hydrogen and carbon monoxide inlet gases. However, in the present work FU_{H2} is preferred, since this descriptor can state more clearly if carbon monoxide is oxidized at a given operating point. As illustrated in Figure S1, a bypass of the fuel gas around the anode is

possible within the ceramic cell housing in the employed setup. Moreover, the cell housing has not been optimized to deliver an equally distributed gas profile across the cell. Thus, the values of the fuel utilization (*FU*) reported in this study are influenced by the setup. However, as the same cell housing is used for all investigated cells, the magnitude of the bypass flow rate is the same in all experiments. Anode and cathode were contacted with nickel and gold meshes, respectively, and gold was used as the sealant between the anode and the cathode side. In all tests, cells were operated with varying fuel mixtures and different H_2S concentrations at a constant total fuel flow rate of 1 L•min^{-1} for each cell. The cathode was operated with air at a constant flow rate of 2 L•min^{-1}. Humidification was carried out by running the gas through a temperature-controlled water bubbler. H_2S was taken from a pressurized H_2S/N_2 (or H_2S/H_2, respectively, for the hydrogen oxidation experiments) bottle containing 150 ppm H_2S.

The cells were briefly heated (3 K/min) to 950 °C for sealing and subsequently reduced at 900 °C. Afterwards, the operating temperature of 850 °C was adjusted. The OCV was checked before starting the tests and confirmed to be higher than 1.22 V at 900 °C in pure hydrogen (1 L•min^{-1}) and air (1 L•min^{-1}) for all investigated cells, assuring proper gas tightness. Electrochemical experiments were carried out in a number of different fuel gas mixtures (Table I). Initially, the sulfur poisoning behavior of the cells was investigated in a H_2/H_2O fuel mixture in order to allow a comparison with recently published findings (mixture number I).[29] Then, two different synthetic reformate gas mixtures were used (mixtures II and IV), that correspond to the equilibrium gas compositions at the operation temperature of 850 °C. The equilibrium gas phase compositions and the theoretical open circuit voltage according to the Nernst voltage were calculated with CANTERA.[55] For both reformate mixtures, experiments of the same cell were also carried out in a reference fuel consisting of H_2, H_2O and N_2 (gas mixtures III and V). Moreover, the sulfur poisoning effect on CO oxidation (mixture VI) and

methane steam reforming (mixture VII) was investigated. All gas phase compositions are listed in Table I.

Table I. Inlet gas phase compositions in the different experiments and indications with which cell they were performed.

Number of fuel gas mixture	H_2	H_2O	CO	CO_2	N_2	CH_4	Ni/YSZ	Ni/CGO
I	97	3	-	-	-	-	Yes	Yes
II	16	14	16	14	40	-	-	Yes
III	32	14	-	-	54		-	Yes
IV	7	7	20	20	46	-	Yes	Yes[a]
V	7	7	-	-	86	-	Yes[a]	Yes[a]
VI	-	-	20	20	60	-	Yes	Yes[a]
VII	16	23	-	-	50	11	-	Yes

[a] Experiments in gas mixtures IV, V and VI were carried out with a different cell from the same batch than the other experiments. However, performance of the commercial Ni/CGO-based SOFC was shown to be highly reproducible.

The conducted experiments include a systematic investigation of the effect of the hydrogen sulfide concentration on the extent of sulfur poisoning on Ni/CGO for the fuel gas mixtures I and II. Therefore, the H_2S concentration was stepwise increased and set to 1, 2, 5, 10, and 20 ppm at each operating point until saturation occurred. After saturation of the last performance drop related to 20 ppm H_2S, its supply was switched off, the gas flow was substituted with pure N_2 (or H_2) and the anode was regenerated until performance had stabilized. This test protocol was repeated at the different current densities i = Open circuit voltage (OCV), 0.25, 0.5 and 0.75 $A \cdot cm^{-2}$. The cells were characterized by means of electrochemical impedance spec-

troscopy at each H_2S concentration. Therefore, an electrochemical workstation (Zahner® PP-240 with Thales software) in a frequency range from 100 mHz to 100 kHz with 8 points per decade was used. The amplitude of the current stimulus was 500 mA and chosen in order to achieve a voltage response not higher than 15 mV. SEM images were recorded with a Zeiss Ultra Plus SEM. Current-voltage characteristics (*i-V* curves) were measured by varying the current by 0.024 A every 2 seconds.

Results and discussion

The main objective of the present study is to establish the effect of hydrogen sulfide on Ni/CGO-based SOFC operating on reformate fuels. In order to allow an isolated examination of the different reforming processes (Eq. 1–5), the following subsections present the investigation of the sulfur poisoning effect on Ni-based anodes operating on different fuels. Firstly, Ni/YSZ and Ni/CGO anodes were characterized in H_2/H_2O fuel systems. In the second subsection, a model reformate containing H_2, H_2O, CO and CO_2 is used as fuel in order to represent realistic operating conditions. Subsequently, in order to answer mechanistic questions the influence of sulfur on electrochemical CO oxidation and lastly, on methane steam reforming is investigated.

Sulfur poisoning in H_2/H_2O systems

The current-voltage characteristics of the two cells in a H_2/H_2O (97/3) fuel gas mixture at 850 °C are shown in Figure S2. Additionally, the recorded results of a second Ni/CGO10-based SOFC ("Ni/CGO-Ref") are depicted as recently published.[29] The Ni/YSZ-based cell reaches 0.63 $A \cdot cm^{-2}$ at 0.7 V, while the Ni/CGO-based cell achieves 0.88 $A \cdot cm^{-2}$ at the same voltage. The analysis of the electrochemical impedance spectra in Figure S4 shows that the higher performance of the Ni/CGO-based cell is mainly due to a decreased ohmic resistance

(0.16 $\Omega \cdot cm^2$ for the Ni/CGO-based cell and 0.25 $\Omega \cdot cm^2$ for the Ni/YSZ-based cell), while the polarization resistance of the two cells is approximately the same (0.23 $\Omega \cdot cm^2$). As the electrolyte has the same phase composition and thickness in both cells, the increased ohmic resistance of the Ni/YSZ-based cells is probably due to the YSZ adhesion layer, which shows a significantly lower ionic conductivity than the CGO10 adhesion layer of the Ni/CGO-based cell.[56] This also reflects in a lower overall performance. The recently characterized cell "Ni/CGO-Ref" even shows a slightly better performance, with a current density of 0.94 $A \cdot cm^{-2}$ at 0.7 V.

Figure S3a shows the systematic variation of the H_2S impurity level between 0 and 20 ppm in the H_2/H_2O fuel for Ni/CGO-based cell operation at 0.5 $A \cdot cm^{-2}$. Analogously, Figure S3b depicts the poisoning of the Ni/YSZ anode between 0 and 20 ppm H_2S. In Figure 1, the corresponding cell voltage drops and the respective increase in area-specific resistance (ASR) are summarized and compared to the cell "Ni/CGO-Ref". Interestingly, the successive sulfur poisoning did not have a significant effect on the cell voltage of the Ni/CGO-based cell and caused a maximum cell voltage drop of only 9 mV. Moreover, the cell voltage recovered quickly back to the initial cell voltage after stopping the hydrogen sulfide supply. Sulfur exposure to Ni/YSZ led to a voltage drop of 172 mV at 20 ppm H_2S and thus, was a lot more severe than for the Ni/CGO cells. This is also reflected in a higher ASR resistance increase for Ni/YSZ. Furthermore, the Ni/YSZ anode showed a significant extent of irreversible degradation and lost 29 mV of cell voltage within only one poisoning cycle (Figure S3b). Regeneration of Ni/YSZ anodes is an extensively investigated topic and the process was frequently shown to extend over hundreds of hours cases and nevertheless, display irreversible degradation in most cases.[4,39,57,58] Thus, the value for the irreversible voltage drop could possibly further diminish with time. However, as recently shown that irreversible long-term degradation mechanism for Ni/YSZ and Ni/CGO is probably the same and related to the anode overpotential.[3,59] The corresponding values are significantly larger for Ni/YSZ, which leads to a signifi-

cant extent of irreversible voltage degradation already for the investigated short poisoning periods.

Impedance spectroscopy measurements for the Ni/YSZ (Figure S4c+d) and Ni/CGO (Figure S4a+b) electrodes with and without addition of 20 ppm hydrogen sulfide have been carried out. The spectra are influenced by sulfur at the respective opposite ends. Ni/YSZ is affected at frequencies between 10^3 and 10^4 Hz and Ni/CGO at frequencies around 1 Hz. This is consistent with earlier studies of these anodes and can be related to the large capacitance of the Ni/CGO anode process.[8,13,29] This behavior originates from the surface double layer on CGO, which is caused by the accumulation of electrons in the space-charge layer of the MIEC.[60,61]

Interestingly, considerable different voltage drops were observed for the two different Ni/CGO anodes. The cell voltage drop of our recently investigated cell "Ni/CGO-Ref" was 47 mV, and therefore more than five times higher than the one in the present study. This also holds true for the increase in ASR resistance and is unexpected in view of the similar overall performance shown in Figure S2. The fivefold higher ASR increase and voltage drop for the "Ni/CGO-Ref" cell could also be reproduced with several different cells from the same batch for both cell types.

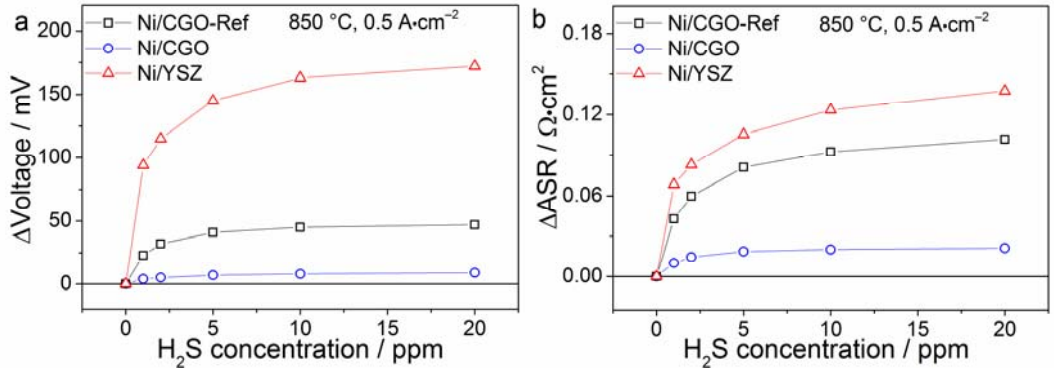

Figure 1: (a) Accumulated voltage drops and (b) accumulated total resistance increase at temperature T = 850 °C, pO_2 = 0.21 atm, pH_2 = 0.97 atm, pH_2O = 0.03 atm, as a function of H_2S concentration.

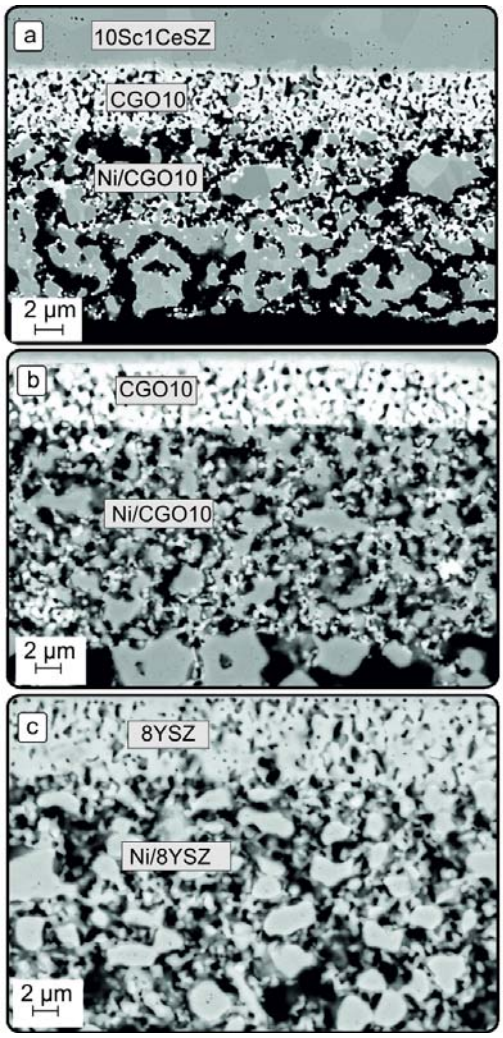

Figure 2. Scanning electron microscopy cross section image of the anodes of (a) the Ni/CGO-based cell, (b) the recently investigated cell "Ni/CGO-Ref" and (c) the Ni/YSZ-based cell. SEM image (a) was supplied by the manufacturer. Therefore, (b) and (c) are recorded at the same magnification, only displaying the adhesion and functional layer.

Impedance spectroscopy measurements at the same condition (OCV, 850 °C, 97 % H_2 and 3 % H_2O in the anode gas) are depicted in Figure S5 and were analyzed by means of equivalent circuit modeling. The results of a complex non-linear square fit showed that the resistance of the low-frequency arc related to anode charge transfer of the Ni/CGO anode (0.2 $\Omega \cdot cm^2$) examined in the present study is smaller than the resistance of the recently investigated cell "Ni/CGO-Ref" (0.28 $\Omega \cdot cm^2$). As the two Ni/CGO-based cells employ different cath-

odes, the respective cathode charge transfer processes lie at different frequencies (Ni/CGO: ~5 Hz, Ni/CGO-Ref: ~100 Hz), which is also evident by the different shape of the impedance spectra. However, despite the difference in frequencies, neither of these processes are part of the low-frequency arc, and thus, the comparison of the low-frequency arc resistance values should be valid since they only comprise the anode charge transfer and the gas conversion/diffusion processes in both cases. However, in general the separation of the different process resistances from impedance spectra of full cells with Ni/CGO anode is complicated, due to the occurrence of the anode charge transfer resistance at low frequencies, which causes its convolution with other processes in many cases. Thus, the derived values above can only be considered as a rough assessment. However, differences in the anode microstructure are also visible on the SEM images of the Ni/YSZ and the two Ni/CGO10 anodes in Figure 2. The microstructure of Ni/CGO is finer and the CGO particles are better distributed than the recently investigated "Ni/CGO-Ref".[29] This could lead to an increased TPB length and a faster charge transfer reaction and therefore also to a higher sulfur resistivity. However, the demonstrated difference in sulfur tolerance between the two different Ni/CGO-based cells is still large for two cells of nominally equivalent cell architecture, despite differences in the anode charge transfer resistance.

In a number of studies, the reason for the high sulfur tolerance of Ni/CGO was speculated to be due to the MIEC characteristics of CGO.[8,10,11] Moreover, in other fundamental studies Ni was shown to only assume the role of a pure electronic conductor during hydrogen oxidation, which would extend the electrochemical reaction zone to the DPB interface.[22] Based on these studies, the sulfur adsorption on the Ni surface would not be expected to have a major influence on SOFC performance. In our recent study, we have speculated that the hydrogen oxidation mechanism on Ni/CGO could be a convolution of a DPB process on the CGO surface and a spillover process at the TPB between Ni/CGO/gas phase. As a consequence, it is possible that the role of the Ni phase in Ni/CGO anodes differs depending on the exact composition of

the electrode, as a function of particle size, triple phase boundary length and other microstructural parameters.

In order to explore the potential of Ni/CGO anodes operated on reformate fuels with sulfur-containing impurities, the more sulfur tolerant Ni/CGO-based cell was chosen for the following electrochemical experiments.

Sulfur poisoning in reformate-fueled systems

Since most commercial SOFC systems so far are operated with an external fuel gas reformer, the present subsection aims to explore sulfur poisoning in more realistic operating conditions with $H_2/H_2O/CO/CO_2/N_2$-based fuels. Therefore, firstly the effect of increasing H_2S concentrations and current density on the performance of a Ni/CGO-based SOFC operated on a synthetic diesel reformate gas mixture is investigated. Subsequently, the reformate fuel ratio of hydrogen in the gas is lowered in order to reach operating points where CO conversion inevitably must occur.

The effect of H_2S concentration and current density on Ni/CGO anodes operated on reformate fuels.— The voltage stability tests over time are illustrated in Figure 3 for gas mixture II (Table I) and at varying current densities of i = 0.25, 0.5 and 0.75 A•cm^{-2}. In all cases, the overall voltage drop increases stepwise along with the hydrogen sulfide concentration. The initial performance drop that is caused by 1 ppm H_2S, is the largest and a further increase of the hydrogen sulfide concentration only leads to smaller performance losses. The sulfur poisoning for all investigated current densities was observed to be completely reversible as full voltage regeneration was achieved after less than 20 h of sulfur-free operation. This behavior is consistent with sulfur poisoning of Ni/CGO anodes in H_2/H_2O fuel systems as we reported recently.[29]

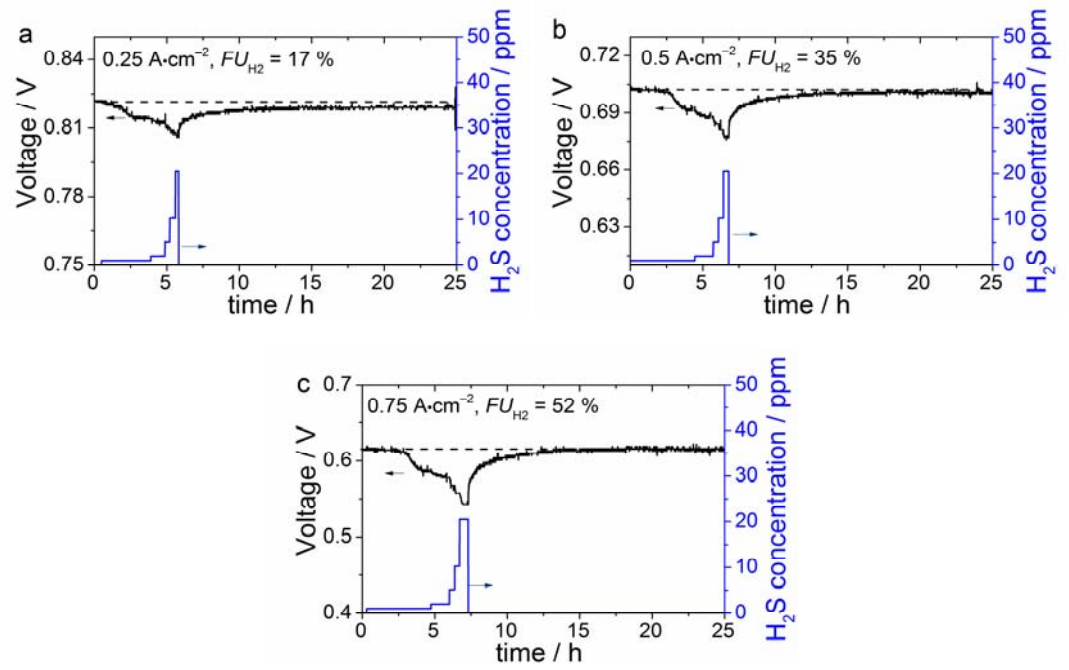

Figure 3: Transient sulfur poisoning tests of the Ni/CGO-based cell fueled with gas mixture II (16 % H_2, 16 % CO, 14 % CO_2, 14 % H_2O, 40 % N_2) and with a stepwise increase of H_2S concentration between 0 – 20 ppm. Operating temperature was 850 °C in all cases. The different current densities a) 0.25 A•cm^{-2}, b) 0.5 A•cm^{-2} and c) 0.75 A•cm^{-2} are shown. The left y-axis shows the voltage behavior (black) during poisoning and recovery phase and the right y-axis the imposed H_2S concentration (blue). Dotted lines indicate the value of the initial voltage before poisoning and are for guiding the eye. Oscillation of the cell voltage due to electrochemical impedance measurements (<15 mV) have been deleted to increase the visibility of the cell voltage evolution.

Overall voltage drops and ASR increase values for all current densities are depicted in Figure 4. For current densities up to 0.5 A•cm^{-2}, all curves show the same characteristic behavior with a drastic change at low H_2S concentrations and a saturation effect at higher concentrations. This behavior is similar to the evolution of the estimated sulfur coverage on Ni, calculated according to a Temkin isotherm.[62] These values are depicted on the right y-axis of Figure 4a for comparison. Interestingly, the poisoning behavior at 0.75 A•cm^{-2} does not follow

this characteristic behavior anymore. At this current density, voltage drop and ASR increase values do not show a saturation effect, but continue increasing. As with increasing current densities the fuel utilization increases (FU_{H2} = 52 %) as well, this behavior could indicate the influence of the inhibited water gas shift reaction or CO oxidation. This could entail mass transport limitations, which lead to a higher sensitivity of the ASR towards small variations of H_2S concentrations. Hence, the observed behavior is likely to be associated with the conversion of CO.

At lower current densities (0.5 A•cm^{-2} and lower), the ASR increase curves show a mitigation effect for the sulfur poisoning test at 0.5 A•cm^{-2}, which shows the lowest ASR increase values. This indicates a general mitigation effect of current density, as already reported before for Ni/YSZ anodes.[63] However, the test at OCV displays lower ASR increase values than the 0.25 A•cm^{-2} test, which is in agreement with our recent study of sulfur poisoning of Ni/CGO anodes in H_2/H_2O fuel gases and indicates that sulfur poisoning at low current densities is governed by its effect on electrochemical hydrogen oxidation.[29] However, the reason for a particular low ASR increase at OCV is still unclear. The highest ASR increase values of the test at 0.75 A•cm^{-2} further suggests that at the corresponding fuel utilization values, the sulfur poisoning of CO conversion has a strong impact on the performance losses.

However, already the ASR increase of 0.06 Ω•cm^2 at 0.5 A•cm^{-2} is considerably larger than the 0.02 Ω•cm^2 for the pure H_2/H_2O fuel system in Figure 1. In order to check if this is a result of the changed pH_2S/pH_2 ratio or of additional resistances due to CO conversion, a reference experiment without CO/CO_2 was conducted. In this poisoning experiment, a fuel gas mixture consisting of 32 % H_2, 14 % H_2O and 54 % N_2 was employed. This corresponds to the reformate with CO replaced by hydrogen and CO_2 replaced by nitrogen and represents the ideal case where all carbon monoxide can readily be converted to hydrogen via the water gas shift reaction. In the corresponding reformate, such high hydrogen contents will not be reached, as it already represents the equilibrium composition at this operating conditions and

conversion of CO into hydrogen via the water gas shift reaction will only occur after hydrogen is consumed by the electrochemical reaction in the first place. However, small variations of the hydrogen partial pressure might occur during operation. Therefore, and as the sulfur coverage on Ni is a function of pH_2S/pH_2,[62] the reference fuel mixture III was considered to represent a "best-case scenario", that is, the highest dilution of H_2S in H_2, with the lowest possible resistance increase.

Judging from the voltage drop and ASR increase, the reference test in the H_2/H_2O fuel system does not result in a considerably lower extent of sulfur poisoning, since these values nearly coincide with the corresponding values for reformate operation. Therefore, it can be concluded that sulfur poisoning on Ni/CGO anodes at low fuel utilization is largely governed by the effect of sulfur on hydrogen oxidation. Thus, the defining parameter responsible for large performance drops in reformate fuel at low current densities is the high pH_2S/pH_2 ratio.

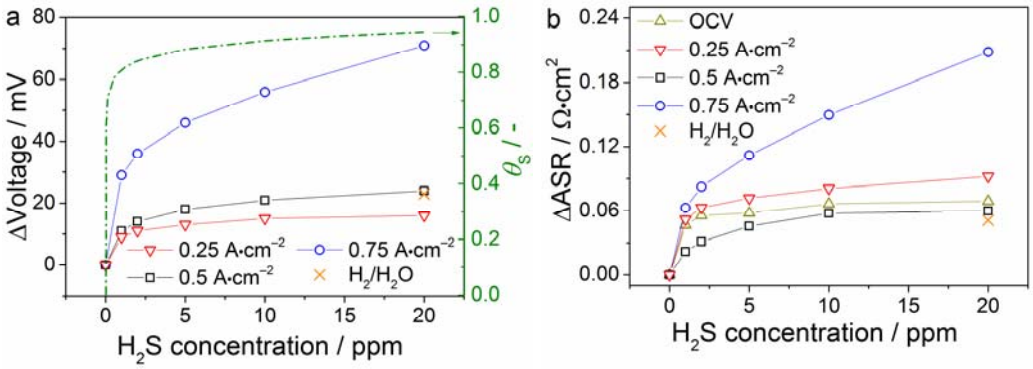

Figure 4: (a) Accumulated voltage drop and (b) accumulated ASR increase for fuel gas mixture II (Table I) at T = 850 °C, as a function of H_2S concentration at different current densities. The H_2/H_2O measurement represents a reference measurement at 0.5 A•cm^{-2} with a fuel consisting of 32 % H_2, 14 % H_2O and 54 % N_2 (orange cross). The right y-axis in a) shows the calculated sulfur coverage on Ni according to the Temkin isotherm derived in Ref.[62]

The introduction of hydrogen sulfide did not cause a voltage change at OCV, thus, the influence of sulfur was captured by electrochemical impedance spectroscopy. The corresponding spectra are illustrated in Figure 5a+b. Additionally, impedance spectra at 0.75 A•cm^{-2} are dis-

played in Figure 5c+d. The Nyquist plots highlight the reported ASR increase, which is a lot more significant for 0.75 A•cm^{-2}. At both current densities, this is reflected by an increase of the imaginary impedance intensity at frequencies between 1–10 Hz. In our recent study, we have identified an anode surface process at this frequency.[29] This process was shown to depend on temperature and anode gas phase composition, and interpreted to correspond to the anode charge transfer reaction. Its low frequency is due to a large chemical capacitance caused by the oxygen non-stoichiometry of CGO. In addition to the influence at this frequency, no further change in the impedance spectra at 0.75 A•cm^{-2} could be observed. However, earlier studies on the sulfur poisoning of the water gas shift reaction on Ni/YSZ anode-supported cells have witnessed a mass transport limitation at similar frequencies ~1 Hz, which overlaps the Ni/CGO anode process in the present study. [5,39,64] This mass transport limitation is caused by the deactivation of the water gas shift reaction, and causes changes in the impedance spectra due to effects on CO/CO_2 diffusion, H_2/H_2O diffusion and gas conversion. In addition to that, the cathode charge transfer process lies in the frequency range between 1 and 10 Hz as well, as the variation of pO_2 effects the impedance response at this frequency range (Figure S6). Therefore, the different processes cannot be separated.

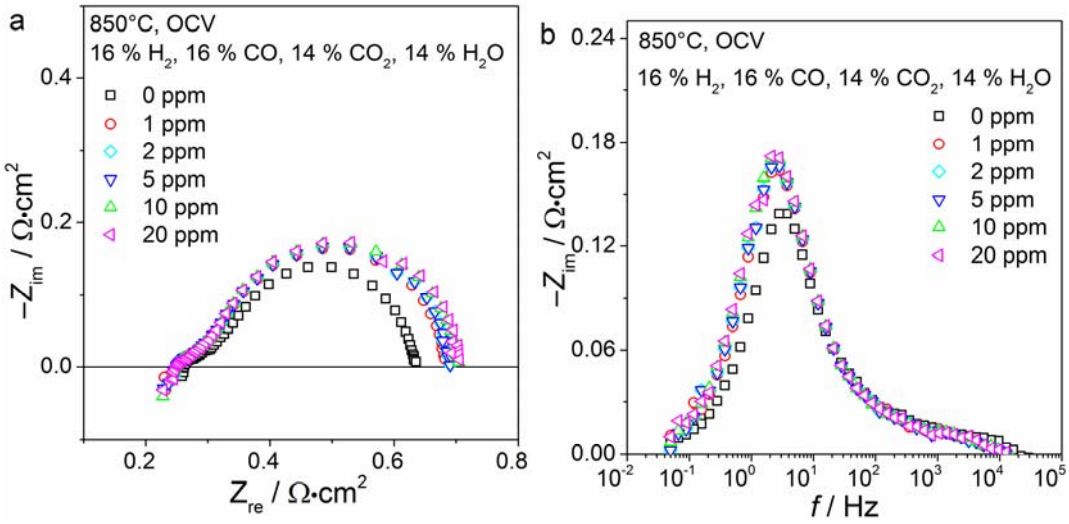

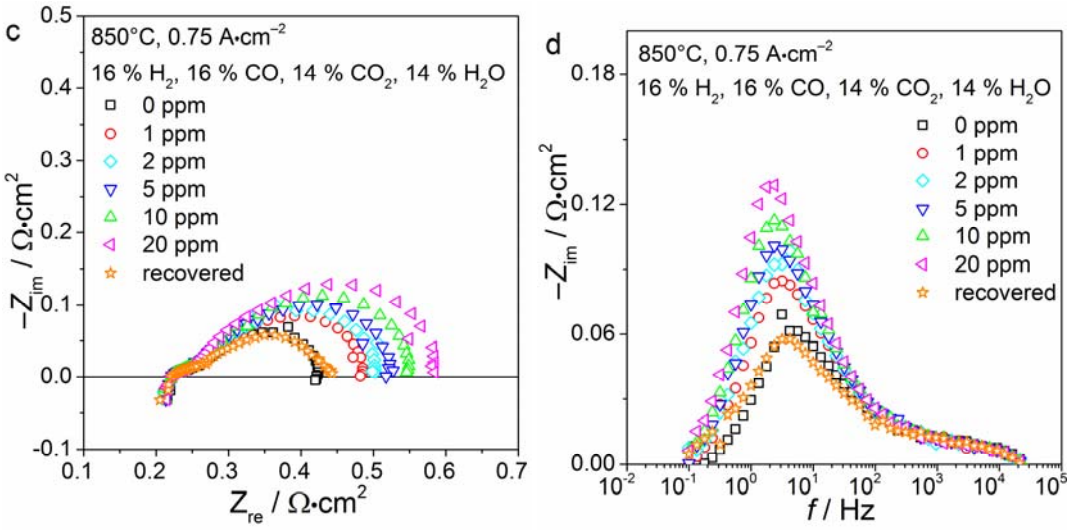

Figure 5: (a) Nyquist and (b) imaginary impedance plot of impedance spectra of the Ni/CGO-based cell recorded for gas mixture II (see Table I) at temperature T = 850 °C, OCV and with different H_2S concentrations between 0 – 20 ppm. (c) and (d) show Nyquist and imaginary impedance plots for i = 0.75 A•cm^{-2}.

The influence of sulfur on carbon monoxide conversion on Ni/CGO and Ni/YSZ.— To obtain further information about the sulfur poisoning behavior of CO conversion on Ni/CGO, a number of *i-V* curves were recorded for both the Ni/CGO and the Ni/YSZ-based cell. The fuel gas was changed to mixture IV (See Table I) in order to make the sulfur influence on the CO oxidation more clearly visible. As the sulfur poisoning on Ni/YSZ was extensively investigated in numerous fuel systems over the years,[5,39,57,64–66] the comparison between the different anodes can give important insights into the different underlying reaction mechanisms. Figure 6a shows the comparison between the data of the reformate-fueled Ni/CGO with and a reference fuel consisting of 7 % H_2, 7 % H_2O and 86 % N_2 (gas mixture V), both of them with and without the addition of 20 ppm H_2S. The reference fuel was chosen in order to represent a system, in which the oxidation of CO is completely disabled and the gases CO and CO_2 are assumed to be inert. Analogous data is depicted for Ni/YSZ in Figure 6b. In reformate fuels, a variety of catalytic reaction can occur on the Ni surface, such as the water gas shift reaction

and the CO oxidation. Since the overall active Ni surface areas of the Ni/YSZ and Ni/CGO-based cells can differ from each other due to the different microstructure, processing and slightly different Ni contents in contact and functional layers, the following analyses rather provides a qualitative than a quantitative comparison.

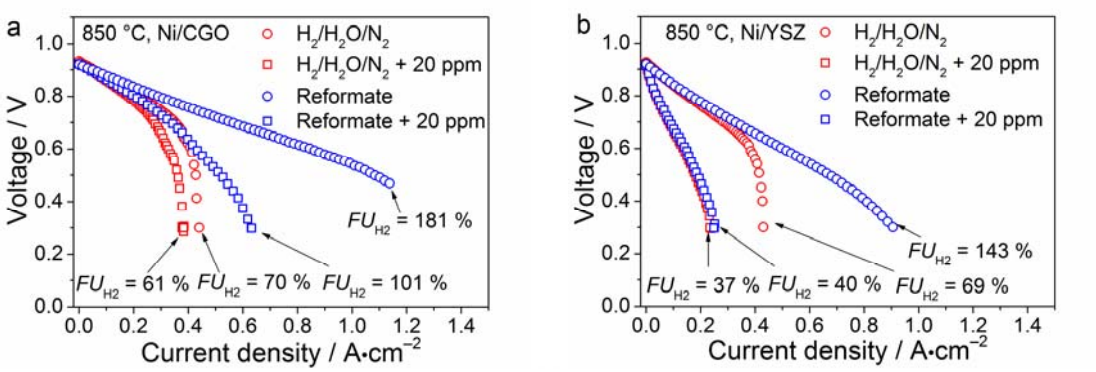

Figure 6: *i-V* curves of the (a) Ni/CGO and the (b) Ni/YSZ-based cell. Experiments were conducted at 850 °C. The reformate consisted of gas mixture IV (blue) containing 7 % H_2, 7 % H_2O, 20 % CO, 20 % CO_2, 46 % N_2 and the reference mixture V (red) containing 7 % H_2, 7 % H_2O, 86 % N_2. *i-V* curves were recorded with (squares) and without (circles) the addition of 20 ppm H_2S.

The Ni/CGO-based cell is operated on a maximum hydrogen utilization of 181 % at a current density of 1.14 A•cm^{-2} and a voltage of 0.47 V. Thus, at this operating point a significant amount of CO is converted. The sulfur poisoning of this anode results in a severe performance loss and only leads to a maximum current density of 0.64 A•cm^{-2} at 0.3 V. The reference fuel consisting of H_2 and H_2O only displays a small performance drop from 0.44 A•cm^{-2} to 0.39 A•cm^{-2}, which again demonstrates the high sulfur tolerance of Ni/CGO anodes towards hydrogen oxidation. The maximum fuel utilization in the case of H_2/H_2O operation reaches around 70 %. Therefore, losses due to bypasses and a non-optimized gas flow profile can amount to up to 30 %. Still, under poisoning conditions a hydrogen utilization of 101 % is obtained with the reformate fuel without reaching the limiting current density. Moreover, the

comparison between the two *i-V* curves under sulfur exposure clearly shows a significant better performance of the reformate-fueled cell. Therefore, it can be concluded that CO conversion is still active under reformate operation and exposure to 20 ppm H_2S.

The Ni/YSZ-based cell fueled with reformate is initially also operated in a regime where CO is oxidized (FU_{H2} = 143 %) and shows a better performance than in the experiment without CO/CO_2. However, after exposure to 20 ppm H_2S the *i-V* curves of both fuel gas mixtures coincide. This is a clear indication that CO conversion is fully deactivated on these cells, implying that both water gas shift reaction and electrochemical CO oxidation are completely blocked under these conditions. Furthermore, these experiments demonstrate that the increased sulfur tolerance of Ni/CGO anodes is not only limited to systems with H_2/H_2O fuel gases, but also extends to reformate operation. However, so far it is unclear if the reason for this increased sulfur tolerance in reformate-operation is the activity of the water gas shift reaction or the electrochemical CO oxidation reaction, or possibly both. Therefore, sulfur poisoning experiments of Ni/CGO and Ni/YSZ in $CO/CO_2/N_2$ fuels are shown in the following subsection.

Sulfur poisoning of electrochemical CO oxidation on Ni/CGO and Ni/YSZ

Similarly to the previous subsection, *i-V* curves were measured in order to assess the effect of sulfur poisoning on CO oxidation. Experiments under the same conditions were carried out for Ni/CGO (Figure 7a) and Ni/YSZ (Figure 7b) with a gas phase composition of 20 % CO, 20 % CO_2 and 60 % N_2 with and without addition of 20 ppm hydrogen sulfide. This is the equilibrium gas composition at 850 °C, thus, catalytic reactions are avoided. Moreover, coke formation at the operating conditions was ensured not to be favorable by thermodynamic calculations. A comparison of the maximum current density at a cell voltage of 0.4 V demonstrates that the Ni/CGO-based cell (0.91 $A \cdot cm^{-2}$) shows a significantly better performance than Ni/YSZ (0.38 $A \cdot cm^{-2}$). Due to different processing conditions and previous poisoning

experiments, which caused irreversible degradation on Ni/YSZ, this difference in performance is no proof for an inherently higher activity of Ni/CGO towards CO oxidation. However, exposure of the two cells to hydrogen sulfide, reveals interesting mechanistic details about the behavior of the electrodes. Sulfur poisoning of Ni/YSZ with 2 ppm H_2S leads to a nearly immediate breakdown of the cell voltage after the beginning of the voltage variation. The maximum achieved current density is 0.002 $A \bullet cm^{-2}$, which clearly illustrates that CO oxidation is fully deactivated under these conditions.

This also leads to the observation of an interesting phenomenon during the sulfur poisoning process at OCV (Figure 8). While the cell voltage of the Ni/CGO-based cell stays constant throughout the experiment, the cell voltage of the Ni/YSZ-based cell quickly drops from 0.922 V over 0.771 V (2 ppm) and 0.727 V (10 ppm) to 0.712 V (20 ppm). After the hydrogen sulfide supply is switched off, the OCV slowly recovers back to the initial value within 24 hours.

So far, an influence of sulfur poisoning on OCV values has only been observed for internal methane steam reforming on Ni/YSZ, since in this case the blockage of the Ni surface hinders CH_4 conversion.[37] Thus, the gas composition is altered during the poisoning process and the Nernst voltage changes. However, this should not be the case for pure CO oxidation since the gas phase composition is already in equilibrium. Another reason for the change in OCV could be the complete blockage of the Ni surface for CO adsorption as it was already indicated in literature.[39] This is consistent with more fundamental studies of Ni(111) surfaces, that indicated that CO adsorption is entirely inhibited for surface coverage higher than 0.3 ML.[67] Recent elementary kinetic modeling studies indeed showed that CO oxidation proceeds via CO adsorption on Ni.[43,68] Hence, complete surface blockage would result in the disappearance of the corresponding electromotive force. Consequently, the OCV must be related to a different galvanic chain. Ni oxidation is a common phenomenon in fuel gases with low hydrogen content. However, in a reference measurement where the entire anode gas supply was substituted with

pure nitrogen, an OCV of 0.655 V was observed. This is consistent with previously reported OCV values for nickel oxidation around 0.7 V.[69] As the observed voltage of the poisoned Ni/YSZ anode is considerably larger, it is likely not to be caused by Ni oxidation. In further experiments (not shown here), the OCV of Ni/YSZ under CO/CO_2 operation was observed to increase with carbon monoxide and decrease with carbon dioxide gas phase concentration after sulfur poisoning. Consequently, the OCV is still associated with a carbon monoxide oxidation process with carbon dioxide as product. Since the OCV is changing only under sulfur exposure, we postulate that carbonyl sulfide (COS) is formed on the surface, which was shown to be the second most thermodynamically stable sulfur-containing species in CO-rich gas phase mixtures.[70] The lowered OCV could then correspond to the following reaction:

$$COS_{Ni} + 3O^{2-} \rightleftharpoons CO_{2,g} + SO_{2,g} + 6e^{-} \quad (6)$$

Furthermore, it was shown that Ni_3S_2 formation can occur for pH_2S/pH_2 values above 10^{-3} (100 ppm).[71] Hence, as hydrogen is absent in gas mixture VI, it is possible that Ni sulfide is created upon anode sulfur exposure which could cause the CO_2 and SO_2 to form via reaction of CO and Ni_3S_2. Since the processes on Ni at OCV occur under equilibrium conditions in the absence of current, Ni sulfide formation can also reasonably be expected on Ni/CGO. Therefore, neither a full Ni surface blockage with sulfur nor Ni sulfide formation can solely explain the different electrode behaviors at OCV. Whatever the underlying mechanism of the OCV decrease in the case of Ni/YSZ is, the negligible maximum current density at 0.4 V shows that the kinetics of the corresponding carbon monoxide oxidation reaction are slow and a concurrent surface reaction like (6) can lead to significant OCV mixed potential formation.

Although the influence of sulfur poisoning of the Ni/CGO electrode on CO oxidation is significant as well and leads to a reduction of the maximum current density to 0.56 $A \cdot cm^{-2}$ at 20 ppm, the CO oxidation process is still active. The impedance spectra in Figure S7 conducted at OCV show a considerable ASR increase after sulfur exposure as well, which is reflected by an increased intensity of the imaginary impedance at around 1 Hz. Thus, carbon monoxide

oxidation on Ni/CGO displays the same relaxation time as hydrogen oxidation (see Fig. S4b). The increase of H_2S concentration from 2 ppm to 20 ppm does not have a significant influence on the maximum current density.

Due to unavailability of water and hydrogen in these experiments, the carbon monoxide must be electrochemically oxidized. This demonstrates that electrochemical CO oxidation on Ni/CGO shows high reaction rates even under severe sulfur exposure and is likely to bear the main responsibility for the comparatively high performance under reformate operation in the previous subsection. Sulfur removal from the Ni surface via SO_2 formation can be excluded to be the reason for the stable voltage of Ni/CGO in Figure 8 due to the absence of current. This shows that the CGO surface is dominating the electrochemial carbon monoxide oxidation at least close to OCV conditions, due to its intrinsic electro-catalytic activity.[12,17–24] Sulfur is able to adsorb on CGO as well, thus, the performance drops observed in Figure 7a might also partly be related to CGO surface poisoning. However, performance drops due to sulfur poisoning on pure CGO anodes were shown to be small, indicating a low sulfur coverage on CGO.[32] This might also be due to a oxidation of CGO-adsorbed sulfur to SO_2.[12,17,72] Moreover, it has been demonstrated that sulfur diffuses into the CGO bulk at high temperatures, at least for cathodic polarization and in single crystal reduced ceria.[33,34] However, so far this diffusion process and SO_2 formation have both not yet been proven to occur in realistic SOFC operating conditions.

Although it does not occur at OCV, sulfur could still be removed from the Ni surface at higher current densities. However, according to DFT calculations the binding energy of CO to the Ni surface is considerably more positive than the one of sulfur, making a preferred sulfur oxidation via oxygen spillover unlikely.[73,74] Nonetheless, the hypothesis of a rapid oxygen spillover from CGO to Ni and a corresponding SO_2 formation cannot definitely be discarded. This would still enable the adsorption of CO on the Ni surface and includes the possibility of an active water gas shift reaction, which could represent the major difference between the two

electrodes. In order to investigate this mechanistic hypothesis, methane steam reforming experiments were carried out and are shown in the next subsection.

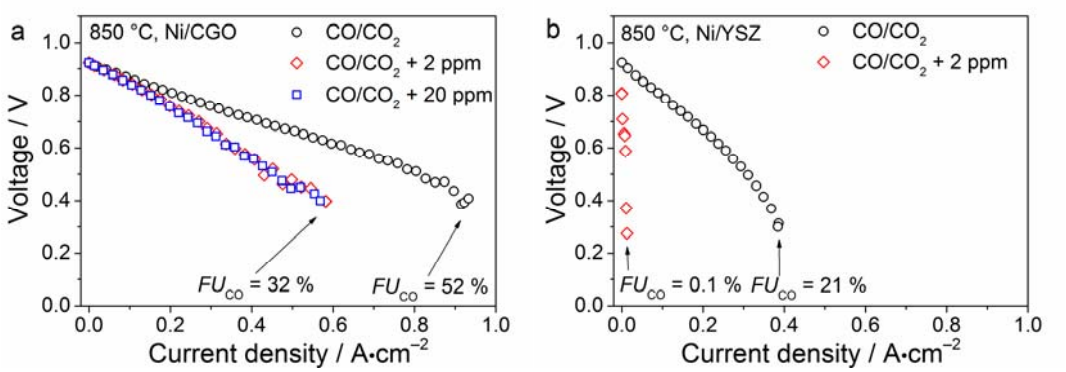

Figure 7: *i-V* curves of the (a) Ni/CGO and the (b) Ni/YSZ-based cell. Experiments were conducted at 850 °C. The fuel gas mixture consisted of gas mixture VI (see Table I). *i-V* curves were recorded with (squares) and without (circles) the addition of 20 ppm H_2S.

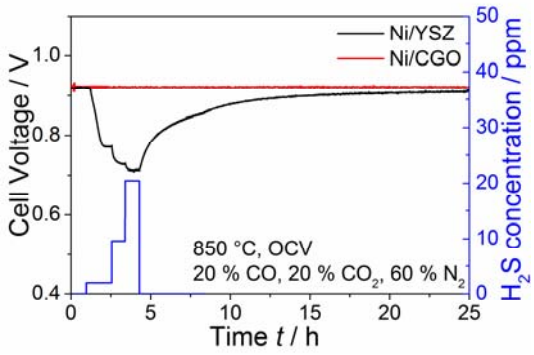

Figure 8: Transient sulfur poisoning tests of the Ni/CGO-based (red) and Ni/YSZ-based (black) cells fueled with gas mixture VI and an H_2S concentration of 20 ppm. The experiment was carried out at 850 °C and OCV. The left y-axis shows the voltage behavior during poisoning and recovery phase and the right y-axis the imposed H_2S concentration (blue).

Sulfur poisoning of Methane Steam Reforming

Methane steam reforming experiments on Ni/CGO were carried out for Ni/CGO at OCV with fuel gas mixture VII (Figure 9). Sulfur poisoning of this anode leads to a fast voltage drop from 0.998 V to 0.908 V at 20 ppm H_2S, which is similar to the behavior observed for Ni/YSZ anodes.[2,4,6,37] The final cell voltage nearly exactly coincides with the theoretical cell

voltage that is obtained under the assumption that no methane is converted (0.907 V). From these experiments, it can be deduced that methane steam reforming on Ni/CGO is fully blocked under these conditions. This is probably related to the sulfur poisoning of the Ni surface since Ni is an effective methane steam reforming catalyst. Since close to 0 % methane conversion could be observed at 20 ppm H_2S, it is also improbable that the CGO surface plays a significant role in the methane reforming process. Although sulfur is able to adsorb on CGO, its coverage is low and therefore is unlikely to block the full surface.[32] Thus, the inactivity of CGO towards methane reforming probably also holds for non-sulfur conditions. This is consistent with investigations that proved that ceria is almost inactive with respect to C-H bond cracking.[75]

Water gas shift reaction and methane steam reforming have been shown to display the same sulfur poisoning behavior on Ni/YSZ anodes with a complete deactivation already at H_2S concentration of about 20 ppm.[2,37,39] In a catalytic study by Kuhn et al., this similar behavior was attributed to the participation of water in both reactions, which results in a more severe poisoning than for catalytic CO oxidation.[76] Moreover, it was suggested that these two catalytic reactions occur on the same active sites.[77] If this analogy is transferred to the Ni/CGO electrode, it can be considered to be highly likely that also the water gas shift reaction is fully deactivated as well for H_2S concentrations as low as 20 ppm.

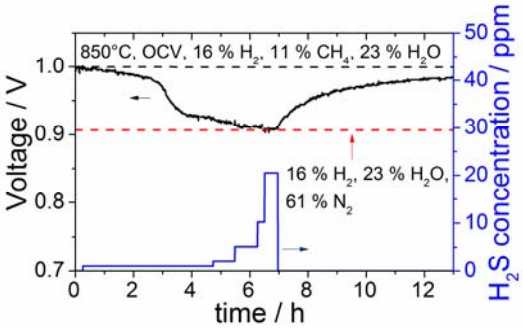

Figure 9: Transient sulfur poisoning tests of the Ni/CGO-based cell fueled with gas mixture VII and with a stepwise increase of H_2S concentration between 0 – 20 ppm. The experiment is carried out at 850 °C and OCV. The left y-axis shows the voltage behavior (black) during

poisoning and recovery phase and the right y-axis the imposed H_2S concentration (blue). The dotted black line indicates the value of the initial voltage before poisoning and is for guiding the eye. Moreover, the dotted red line represents the theoretical Nernst voltage of a gas mixture with 16 % H_2, 23 % H_2O and 61 % N_2. The oscillation of the cell voltage in the figures is caused by electrochemical impedance measurements that were recorded after the saturation of each performance drop. Oscillation of the cell voltage due to electrochemical impedance measurements (<15 mV) have been deleted to increase the visibility of the cell voltage evolution.

Discussion of the effect of sulfur poisoning on Ni/CGO under reformate operation

The experiments in the present study have clearly demonstrated that the high sulfur tolerance of Ni/CGO anodes is not only limited to hydrogen oxidation, but also extends to the oxidation of carbon monoxide. As explained earlier, hypothetic explanations of the high sulfur tolerance of Ni/CGO include the inherent electrocatalytic activity of CGO,[19–24] the oxidation of nickel-adsorbed sulfur to SO_2 involving an oxygen spillover from CGO to Ni,[8,12,32] and sulfur diffusion from the surface to the CGO bulk phase.[33,34] However, based on the presented experiments, we consider the first explanation to be the most likely one. The electrochemical CO oxidation at the TPB, methane steam reforming and the water gas shift reaction seem to be fully deactivated due to nickel-adsorbed sulfur, thus, the electro-catalytic activity of CGO is the reason for continued carbon monoxide oxidation.

A schematic illustration of the proposed underlying mechanism is depicted in Figure 10a+b. It is likely that under sulfur-free operation, the water gas shift reaction on Ni (Eq. (3)) is the dominating pathway for CO conversion into hydrogen and CO_2 due to its rapid kinetics.[78] After sulfur exposure, the water gas shift reaction on nickel is probably fully deactivated for H_2S concentration of approximately 20 ppm, which is concluded based on the analogy between WGS and MSR reaction.[39,76] As the nickel surface is likely to be completely blocked

for CO adsorption, an electrochemical oxidation of CO on Ni at the TPB via oxygen spillover as described by Eq. 7 is also unlikely.

$$CO_{Ni} + O^{2-}_{CGO} \rightleftharpoons CO_{2,Ni} + 2e^- \quad (7)$$

Instead, CO oxidation then proceeds via an electrochemical pathway on the CGO surface:

$$CO_{(g)} + O^{2-}_{CGO} + Ce^{4+} \rightleftharpoons CO_{2,(g)} + Ce^{3+} + (CGO), \quad (8)$$

where (CGO) represents a free active surface site on CGO. During the reaction, similar to hydrogen oxidation,[27,79] the surface cerium atoms change their valence state from Ce^{4+} to Ce^{3+}.[49] Under reformate operation and sulfur exposure, carbon monoxide oxidation on CGO allows higher fuel utilization values than on Ni/YSZ anodes. Although this surface charge transfer process still proceeds under sulfur exposure, the significant poisoning of pure CO oxidation on Ni/CGO (Figure 7a) indicates that the oxidation at the TPB (Eq. 7) probably occurs with a faster reaction rate in sulfur-free fuel gases.

While electrochemical CO oxidation is often completely neglected in SOFC modeling literature,[6,80,81] the present study shows that this is not the case for Ni/CGO anodes under sulfur exposure since CO can also be electrochemically oxidized on the CGO surface. The possibility of high CO oxidation rates on doped ceria was already indicated earlier.[10,48,49] Recently, it was reported that CGO model electrodes with CGO nanoparticles can even show higher electrocatalytic activity towards CO/CO_2 than towards H_2/H_2O reactions.[48] CO oxidation on CGO was shown to probably proceed via a Mars-van-Krevelen mechanism.[82] Therefore, the global reaction described in Eq. 8 could possibly be further resolved into an oxygen discharge (Eq. 9)[83] and a catalytic CO oxidation reaction (Eq. 10).

$$O^{2-}_{CGO,b} + 2Ce^{4+} \rightleftharpoons 2Ce^{3+} + O_{CGO} \quad (9)$$

$$CO_{(g)} + O_{CGO} \rightleftharpoons CO_{2,(g)} + (CGO) \quad (10)$$

At a lower temperatures of 500 °C, Feng et al. suggested CO oxidation on CGO to occur via a carbonate molecule.[49] However, this might change at higher temperatures. Thus, the dominat-

ing mechanism of CO oxidation on ceria is still unclear.

In general, the rates of methane steam reforming and the water gas shift reaction on Ni depend on the sulfur coverage to the third power $(1–\theta_S)^3$ and thus, are more severely affected than the rate of the electrochemical hydrogen oxidation on Ni/YSZ that follows the dependency $(1-\theta_S)$.[7,84,85] Russner et al. even showed a stronger deactivation of the WGS than the MSR reaction.[86] Thus, hydrogen oxidation can still be active at operating conditions where methane steam reforming and water gas shift reaction are fully deactivated.

Ceria is easily oxidized by H_2O as shown in literature.[87] This is also reflected by the dependence of the capacitance on the operating conditions (pO_2, T).

$$H_2O + 2Ce^{3+} \rightleftharpoons 2Ce^{4+} + O_{CGO} + H_2 \quad (11)$$

Since reaction 7 was shown to be possible on the CGO surface via experiments in CO/CO_2 fuels, the combination of the reactions (7) + (11) is the water gas shift reaction, which proceeds essentially via a redox mechanisms. This was already proposed in the literature for ceria-supported precious metal.[88]

$$CO_{(g)} + O_{CGO} \rightleftharpoons CO_{2,(g)} + (CGO) \quad (12)$$

In this case, the oxygen necessary for the reaction can also be supplied from the water in the gas phase. Accordingly, at the present high operating conditions the water gas shift reaction should still be active due to the high activity of CGO towards CO oxidation.

Furthermore, as we proposed recently, on Ni/CGO hydrogen could either be dissociated on Ni or also be directly oxidized on CGO.[29] Hydrogen oxidation on the CGO surface in turn, could also be poisoned by sulfur, however, only to a small degree, possibly due to SO_2 formation on the CGO surface (not on nickel). Based on the observed differences in sulfur tolerance for nominally equivalent anodes in Figure 1, it is possible that the TPB and DPB processes are competitive and the prevailing pathway varies depending on the microstructure.

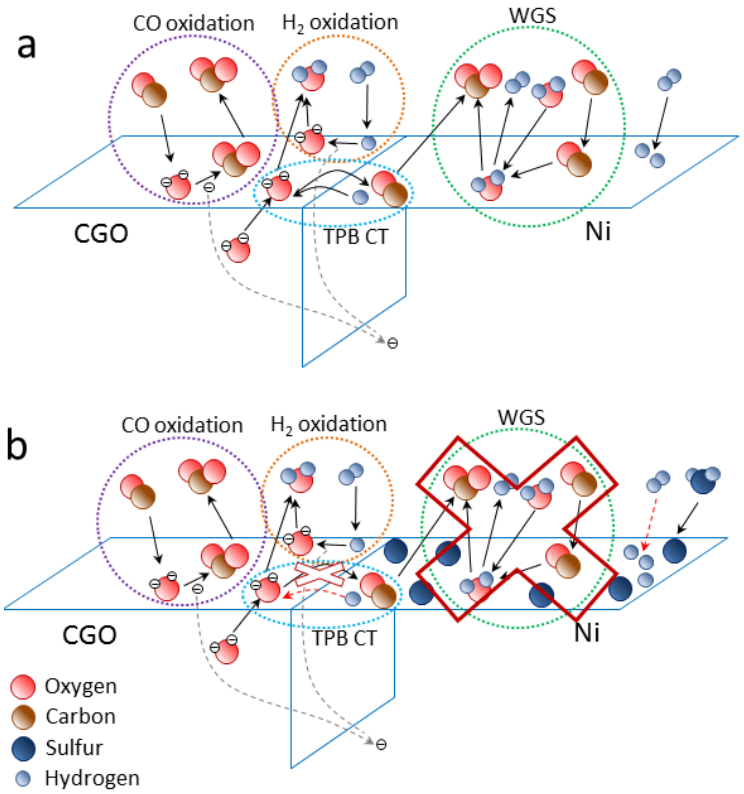

Figure 10: Schematic illustration of the reaction mechanism of the fuel oxidation (a) without and (b) with sulfur poisoning on Ni/CGO-based anodes operated on reformate mixtures. Reactions fully blocked by sulfur are signified by a red cross. Reactions that still proceed, but at a lower reaction rate are illustrated with dashed red lines. Dashed grey lines indicate the pathway of electron transfer. Dashed circles signify the water gas shift reaction (WGS), the charge transfer reactions at the triple phase boundary (TPB CT), electrochemical oxidation on CGO, and electrochemical hydrogen oxidation on CGO.

Summary and conclusions

The sulfur poisoning behavior of ESC with Ni/CGO10 anodes operating on reformate fuels was investigated by means of current-voltage characteristics and electrochemical impedance spectroscopy. In order to draw mechanistic conclusions, a variety of different fuels including methane and carbon monoxide-containing reformates were used and a comparison to Ni/YSZ-based SOFC was carried out. It was revealed that the poisoning behavior is mainly governed by a hindered hydrogen oxidation reaction at low current densities in $H_2/H_2O/CO/CO_2$ fuel

gas mixtures. At higher current densities, the poisoning becomes more pronounced, indicating a particularly severe poisoning effect on the carbon monoxide conversion reactions. However, the ability of Ni/CGO anodes to convert CO at H_2S concentration up to 20 ppm was demonstrated, which was shown not to be the case for Ni/YSZ. The sulfur poisoning behavior of Ni/CGO anodes was reversible for the investigated short exposure times. Sulfur poisoning experiments of methane steam reforming suggest that the Ni surface is entirely blocked and the water gas shift reaction is fully deactivated. However, electrochemical CO oxidation on the CGO surface was shown to be still active for hydrogen sulfide concentrations of 20 ppm. The presented results clearly demonstrate that the high sulfur tolerance of Ni/CGO is not only limited to H_2/H_2O fuel systems, but also extends to CO-containing gases.

Supporting Information

Illustration of cell housing; *i-V* curves; Transient sulfur poisoning tests in H_2/H_2O fuel; EIS of sulfur poisoning in H_2/H_2O fuel; EIS comparison of both Ni/CGO-based cells; EIS with influence of pO_2; EIS with influence of sulfur poisoning in CO/CO_2 fuels

Acknowledgments

We gratefully acknowledge financial support from the German Ministry of Education and Research (BMBF) within the framework of the project "SOFC-Degradation: Analyse der Ursachen und Entwicklung von Gegenmaßnahmen" via grant number 03SF0494C. Dr. Mihails Kusnezoff and Dr. Nikolai Trofimenko of the Fraunhofer Institute for Ceramic Technologies and Systems (IKTS) are gratefully acknowledged for the supply of cells. We acknowledge Mike Steilen for help with Cantera simulations. Furthermore, we would like to thank Dr. Vitaliy Yurkiv and Dr. Norbert Wagner for valuable fundamental discussions.

References

(1) Riegraf, M.; Schiller, G.; Costa, R.; Friedrich, K. A.; Latz, A.; Yurkiv, V. *J. Electrochem. Soc.* **2014**, *162*, F65–F75.

(2) Hagen, A.; Rasmussen, J. F. B.; Thyden, K. *J. Power Sources* **2011**, *196*, 7271–7276.

(3) Hauch, A.; Hagen, A.; Hjelm, J.; Ramos, T. *J. Electrochem. Soc.* **2014**, *161*, F734–F743.

(4) Hagen, A.; Johnson, G. B.; Hjalmarsson, P. *J. Power Sources* **2014**, *272*, 776–785.

(5) Kromp, A.; Dierickx, S.; Leonide, A.; Weber, A.; Ivers-Tiffée, E. *J. Electrochem. Soc.* **2012**, *159*, B597–B601.

(6) Riegraf, M.; Yurkiv, V.; Schiller, G.; Costa, R.; Latz, A.; Friedrich, K. A. *J. Electrochem. Soc.* **2015**, *162*, 1324–1332.

(7) Hansen, J. B.; Rostrup-Nielsen, J. *Handb. Fuel Cells* **2010**, *6*, 1.

(8) Kavurucu Schubert, S.; Kusnezoff, M.; Michaelis, A.; Bredikhin, S. I. *J. Power Sources* **2012**, *217*, 364–372.

(9) Trembly, J. P.; Marquez, A. I.; Ohrn, T. R.; Bayless, D. J. *J. Power Sources* **2006**, *158*, 263–273.

(10) Ouweltjes, J. P.; Aravind, P. V.; Woudstra, N.; Rietveld, G. *J. Fuel Cell Sci. Technol.* **2006**, *3*, 495.

(11) Aravind, P. V.; Ouweltjes, J. P.; Woudstra, N.; Rietveld, G. *Electrochem. Solid-State Lett.* **2008**, *11*, B24–B28.

(12) Xu, C.; Gansor, P.; Zondlo, J. W.; Sabolsky, K.; Sabolsky, E. M. *J. Electrochem. Soc.* **2011**, *158*, B1405–B1416.

(13) Zhang, L.; Jiang, S. P.; He, H. Q.; Chen, X.; Ma, J.; Song, X. C. *Int. J. Hydrogen Energy* **2010**, *35*, 12359–12368.

(14) Lohsoontorn, P.; Brett, D. J. L.; Brandon, N. P. *J. Power Sources* **2008**, *183*, 232–239.

(15) Mai, A.; Iwanschitz, B.; Weissen, U.; Denzler, R.; Haberstock, D.; Nerlich, V.; Schuler, A. *ECS Trans.* **2009**, *25(2)*, 149–158.

(16) Kusnezoff, M.; Trofimenko, N.; Müller, M.; Michaelis, A. *Materials* **2016**, *9*, 906–914.

(17) Niakolas, D. K. *Appl. Catal., A* **2014**, *486*, 123–142.

(18) Neofytidis, C.; Athanasiou, M.; Neophytides, S. G.; Niakolas, D. K. *Top. Catal.* **2015**, *58* (18-20), 1276–1289.

(19) Nakamura, T.; Kobayashi, T.; Yashiro, K.; Kaimai, A.; Otake, T.; Sato, K.; Mizusaki, J.; Kawada, T. *J. Electrochem. Soc.* **2008**, *155*, B563–B569.

(20) Iwanschitz, B.; Sfeir, J.; Mai, A.; Schütze, M. *J. Electrochem. Soc.* **2010**, *157*, B269–B278.

(21) Papaefthimiou, V.; Shishkin, M.; Niakolas, D. K.; Athanasiou, M.; Law, Y. T.; Arrigo, R.; Teschner, D.; Hävecker, M.; Knop-Gericke, A.; Schlögl, R.; Ziegler, T.; Neophytides, S. G.; Zafeiratos, S. *Adv. Energy Mater.* **2013**, *3*, 762–769.

(22) Chueh, W. C.; Hao, Y.; Jung, W.; Haile, S. M. *Nat. Mater.* **2011**, *11*, 155–161.

(23) Zhang, C.; Grass, M. E.; McDaniel, A. H.; DeCaluwe, S. C.; El Gabaly, F.; Liu, Z.; McCarty, K. F.; Farrow, R. L.; Linne, M. A.; Hussain, Z.; Jackson, G. S.; Bluhm, H.; Eichhorn, B. W. *Nat. Mater.* **2010**, *9*, 944–949.

(24) Chueh, W. C.; Haile, S. M. *Phys. Chem. Chem. Phys.* **2009**, *11*, 8144–8148.

(25) Lu, C.; Worrell, W. L.; Vohs, J. M.; Gorte, R. J. *J. Electrochem. Soc.* **2003**, *150*, A1357–A1359.

(26) He, H.; Gorte, R. J.; Vohs, J. M. *Electrochem. Solid-State Lett.* **2005**, *8*, A279–A280.

(27) Feng, Z. A.; El Gabaly, F.; Ye, X.; Shen, Z.-X.; Chueh, W. C. *Nat. Commun.* **2014**, *5*, 1–9.

(28) Decaluwe, S. C.; Grass, M. E.; Zhang, C.; Gabaly, F. El; Bluhm, H.; Liu, Z.; Jackson, G. S.; McDaniel, A. H.; McCarty, K. F.; Farrow, R. L.; Linne, M. A.; Hussain, Z.; Eichhorn, B. W. *J. Phys. Chem. C* **2010**, *114*, 19853–19861.

(29) Riegraf, M.; Yurkiv, V.; Costa, R.; Schiller, G.; Friedrich, K. A. *ChemSusChem* **2017**, *10*, 587–599.

(30) Yun, J. W.; Ham, H. C.; Kim, H. S.; Song, S. A.; Nam, S. W.; Yoon, S. P. *J. Electrochem. Soc.* **2012**, *160*, F153–F161.

(31) Lohsoontorn, P.; Brett, D. J. L.; Brandon, N. P. *J. Power Sources* **2008**, *175*, 60–67.

(32) Mirfakhraei, B.; Paulson, S.; Thangadurai, V.; Birss, V. *J. Power Sources* **2013**, *243*, 95–101.

(33) Mullins, D. R.; McDonald, T. S. *Surf. Sci.* **2007**, *601*, 4931–4938.

(34) Gerstl, M.; Nenning, A.; Iskandar, R.; Rojek-Wöckner, V.; Bram, M.; Hutter, H.; Opitz, A. K. *Materials* **2016**, *9*, 649–682.

(35) Smith, T. R.; Wood, A.; Birss, V. I. *Appl. Catal., A* **2009**, *354*, 1–7.

(36) Yoshizumi, T.; Uryu, C.; Oshima, T.; Shiratori, Y.; Ito, K.; Sasaki, K. *ECS Trans.* **2011**, *35*, 1717–1725.

(37) Rasmussen, J. F. B.; Hagen, A. *Fuel Cells* **2010**, *10*, 1135–1142.

(38) Li, T. S.; Xu, M.; Gao, C.; Wang, B.; Liu, X.; Li, B.; Wang, W. G. *J. Power Sources* **2014**, *258*, 1–4.

(39) Hagen, A. *J. Electrochem. Soc.* **2012**, *160*, F111–F118.

(40) Shiratori, Y.; Ijichi, T.; Oshima, T.; Sasaki, K. *Int. J. Hydrogen Energy* **2010**, *35*, 7905–7912.

(41) Hecht, E. S.; Gupta, G. K.; Zhu, H.; Dean, A. M.; Kee, R. J.; Maier, L.; Deutschmann, O. *Appl. Catal., A* **2005**, *295*, 40–51.

(42) Kee, R. J.; Zhu, H.; Goodwin, D. G. *Proc. Combust. Inst.* **2005**, *30*, 2379–2404.

(43) Yurkiv, V.; Utz, A.; Weber, A.; Ivers-Tiffée, E.; Volpp, H. R.; Bessler, W. G. *Electrochim. Acta* **2012**, *59*, 573–580.

(44) Utz, A.; Leonide, A.; Weber, A.; Ivers-Tiffée, E. *J. Power Sources* **2011**, *196*, 7217–7224.

(45) Holtappels, P.; Haart, L. G. J. D. E.; Stimming, U.; Vinke, I. C.; Mogensen, M. *J. Appl. Electrochem.* **1999**, *29*, 561–568.

(46) Matsuzaki, Y.; Yasuda, I. *J. Electrochem. Soc.* **2000**, *147*, 1630–1635.

(47) He, H. P.; Wood, A.; Steedman, D.; Tilleman, M. *Solid State Ionics* **2008**, *179*, 1478–1482.

(48) Graves, C.; Chatzichristodoulou, C.; Mogensen, M. B. *Faraday Discuss.* **2010**, *4*, 1166–1169.

(49) Feng, Z. A.; Machala, M. L.; Chueh, W. C. *Phys. Chem. Chem. Phys.* **2015**, *17*, 12273.

(50) Goodenough, J. B.; Huang, Y.-H. *J. Power Sources* **2007**, *173* (1), 1–10.

(51) Souentie, S.; Athanasiou, M.; Niakolas, D. K.; Katsaounis, A.; Neophytides, S. G.;

Vayenas, C. G. *J. Catal.* **2013**, *306*, 116–128.

(52) Neofytidis, C.; Dracopoulos, V.; Neophytides, S. G.; Niakolas, D. K. *Catal. Today* **2017**, *In Press*.

(53) Trofimenko, N.; Kusnezoff, M.; Michaelis, A. *ECS Trans.* **2011**, *35 (1)*, 315.

(54) Hoerlein, M. P.; Schiller, G.; Tietz, F.; Friedrich, K. A. *ECS Trans.* **2015**, *68*, 3553–3561.

(55) Goodwin, D. Cantera: An object-oriented software toolkit for chemical kinetics, thermodynamics, and transport processes, Caltech, Pasadena, http://code.google.com/p/cantera, (2009).

(56) Fergus, J. W. *J. Power Sources* **2006**, *162* (1), 30–40.

(57) Rasmussen, J. F. B.; Hagen, A. *J. Power Sources* **2009**, *191*, 534–541.

(58) Zha, S.; Cheng, Z.; Liu, M. *J. Electrochem. Soc.* **2007**, *154*, B201–B208.

(59) Riegraf, M.; Costa, R.; Schiller, G.; Friedrich, K. A. *ECS Trans.* **2017**, *78* (1), 1285–1291.

(60) Chueh, W. C.; Haile, S. M. *Annu. Rev. Chem. Biomol. Eng.* **2012**, *3*, 313–341.

(61) Fleig, J. *Phys. Chem. Chem. Phys.* **2005**, *7*, 2027–2037.

(62) Alstrup, I.; Rostrup-Nielsen, J. R. J.; Røen, S. *Appl. Catal.* **1981**, *1*, 303–314.

(63) Cheng, Z.; Zha, S.; Liu, M. *J. Power Sources* **2007**, *172* (2), 688–693.

(64) Weber, A.; Dierickx, S.; Kromp, A.; Ivers-Tiffée, E. *Fuel Cells* **2013**, *13*, 487–493.

(65) Sasaki, K.; Susuki, K.; Iyoshi, A.; Uchimura, M.; Imamura, N.; Kusaba, H.; Teraoka, Y.; Fuchino, H.; Tsujimoto, K.; Uchida, Y.; Jingo, N. *J. Electrochem. Soc.* **2006**, *153*, A2023–A2030.

(66) Matsuzaki, Y. *Solid State Ionics* **2000**, *132*, 261–269.

(67) Erley, W.; Wagner, H. *J. Catal.* **1978**, *53*, 287–294.

(68) Yurkiv, V.; Starukhin, D.; Volpp, H.-R.; Bessler, W. G. *J. Electrochem. Soc.* **2011**, *158*, B5–B15.

(69) Neidhardt, J.; Henke, M.; Bessler, W. *ECS Trans.* **2011**, *35*, 1621–1629.

(70) Sasaki, K. *J. Fuel Cell Sci. Technol.* **2008**, *5*, 031212–031216.

(71) Bartholomew, C. H.; Agrawal, P. K.; Katzer, J. R. *Adv. Catal.* **1982**, *31*, 135–242.

(72) Lim, D.-H.; Kim, H. S.; Yoon, S. P.; Han, J.; Yoon, C. W.; Choi, S. H.; Nam, S. W.; Ham, H. C. *Phys. Chem. Chem. Phys.* **2014**, *16* (22), 10727.

(73) Catapan, R. C.; Oliveira, A. A. M.; Chen, Y.; Vlachos, D. G. *J. Phys. Chem. C* **2012**, *116*, 20281–20291.

(74) Alfonso, D. R. *Surf. Sci.* **2008**, *602*, 2758–2768.

(75) Marina, O. A.; Mogensen, M. *Appl. Catal., A* **1999**, *189*, 117–126.

(76) Kuhn, J. N.; Lakshminarayanan, N.; Ozkan, U. S. *J. Mol. Catal. A: Chem.* **2008**, *282*, 9–21.

(77) Rostrup-Nielsen, J. R.; Hansen, J. B.; Helveg, S.; Christiansen, N.; Jannasch, A. K. *Appl. Phys. A: Mater. Sci. Process.* **2006**, *85*, 427–430.

(78) Kromp, A.; Leonide, A.; Weber, A.; Ivers-Tiffée, E. *J. Electrochem. Soc.* **2011**, *158*, B980–B989.

(79) Chueh, W. C.; McDaniel, A. H.; Grass, M. E.; Hao, Y.; Jabeen, N.; Liu, Z.; Haile, S. M.; McCarty, K. F.; Bluhm, H.; El Gabaly, F. *Chem. Mater.* **2012**, *24*, 1876–1882.

(80) Yurkiv, V. *Electrochim. Acta* **2014**, *143*, 114–128.

(81) Aguiar, P.; Adjiman, C. S.; Brandon, N. P. *J. Power Sources* **2004**, *138*, 120–136.

(82) Aneggi, E.; Llorca, J.; Boaro, M.; Trovarelli, A. *J. Catal.* **2005**, *234*, 88–95.

(83) Yurkiv, V.; Costa, R.; Ilhan, Z.; Ansar, A.; Bessler, W. G. *J. Electrochem. Soc.* **2014**, *161*, F480–F492.

(84) Hansen, J. B. *Electrochem. Solid-State Lett.* **2008**, *11*, B178–B180.

(85) Rostrup-Nielsen, J. R.; Sehested, J.; Norskov, J. K. *Adv. Catal.* **2002**, *47*, 65–139.

(86) Russner, N.; Geisler, H.; Dierickx, S.; Weber, A.; Ivers-Tiffée, E. *ECS Trans.* **2017**, *78(1)* (1), 2673–2682.

(87) Luo, T.; Gorte, R. J. *Catal. Letters* **2003**, *85*, 139–146.

(88) Gorte, R. J.; Zhao, S. *Catal. Today* **2005**, *104* (1), 18–24.